sustainability

MDPI

Article

Study on the Deformation Mechanism of Reservoir Landslides Considering Rheological Properties of the Slip Zone Soil: A Case Study in the Three Gorges Reservoir Region

Chun Li [1], Huiming Tang [2,*] and Yankun Wang [2]

[1] School of Port and Transportation Engineering, Zhejiang Ocean University, Zhoushan 316022, China; chunli@zjou.edu.cn
[2] Faculty of Engineering, China University of Geosciences, Wuhan 430074, China; yankun_wang@cug.edu.cn
* Correspondence: tanghm@cug.edu.cn

Received: 22 June 2020; Accepted: 5 August 2020; Published: 10 August 2020

Abstract: Reservoir water level fluctuation is one of the main extrinsic factors that could change the stress field in landslides, as well as the mechanical strength of geomaterials, hence affecting the deformation and stability of landslides. The largest reservoir landslide in the Three Gorges Reservoir area was selected for a case study. The impact of reservoir water level fluctuation is represented by the dynamic change in the underground seepage field and was thereby analyzed with numerical modeling. The deformation behavior considering the rheological properties of the slip zone soil was studied. The sudden change in the displacement–time curve was selected as the failure criterion for the investigated landslide. The evolution process of the accelerated deformation stage was divided into slow acceleration, fast acceleration, and rapid acceleration stages. The Huangtupo landslide is characterized by a retrogressive landslide and is currently in the creep deformation stage; the deformation mechanism and deformation characteristics are closely related to the reservoir water level fluctuation. Research was carried out by means of field investigation, in situ monitoring, and numerical simulation to provide a true and reliable result for stability evaluation.

Keywords: reservoir landslide; deformation mechanism; landslide seepage field; rheological property

1. Introduction

Landslides tend to happen under the coupled effects of intrinsic-like rheological behavior and extrinsic factors, such as rainfall, earthquakes, and human activities [1,2]. For the Three Gorges Reservoir, the water level in the upper stream of the Yangtze River fluctuates between 145 m and 175 m annually, causing high hydrodynamic pressure and dynamic variations in seepage water pressure, resulting in landslides [3–5]. Some ancient landslides in the reservoir area have been reactivated, and many potential new landslides will be triggered during the service life of the reservoir [6–8]. Deformation characteristics and triggering mechanisms are closely related to reservoir water level fluctuations. The evolution and formation mechanism of three large-scale landslides in the Three Gorges Reservoir Area (TGRA) were thoroughly investigated, and it is found that many features associated with landslides were caused by slow, downslope gravitational processes before landslide failure [9]. The long-term deformation pattern of an ancient landslide with a planar sliding surface in the TGRA was found to be deeply connected with periodic fluctuations in the reservoir water level [10]. The failure of these landslides is strictly influenced by the increase in pore water pressure and the consequent reduction in mean effective stress and is considered a complex slope instability phenomenon since the landslides exhibit distinct kinematic characteristics during the failure, post-failure, and propagation

stages [11–14]. Lots of research achievements on deformation characteristics and failure pattern respect to rainfall and reservoir water level have been obtained, for example, the evolution characteristics of the Huangtupo landslide based on in-situ tunneling and monitoring data were fully introduced, that rapid changes of reservoir water level has a huge influence on the landslide stability [15,16]. Once the relationship between the deformation characteristics and rainfall, or reservoir water level was found, the landslide prediction model can be established [17–19].

Generally, most rheology studies are focused on remolded soil samples, in which coarse particles are eliminated artificially due to the difficulty in abstracting undisturbed slip zone soil from underground [20–23]. However, coarse particles have been shown to have a significant impact on the soil mechanical strength and its deformation [24–27]. As the weakest layer controlling landslide stability, the rheological property of slip zone soil considering its original internal structure requires additional investigation to provide a more reliable and precise result for the evaluation of deformation and stability of landslides [28]. However, limited studies on this aspect have been carried out. Methodologies of previous researches were mainly the numerical simulation method, which seems insufficient without actual deformation data. In addition to this, few studies were focused on landslide creep deformation since such approaches require performing long-term analysis and thus require multi-annual records of time-series.

In this study, the rheological behavior of undisturbed slip zone soil was taken into account, to get a comprehensive understanding of the deformation mechanism, as well as the influence of reservoir water level on long-term deformation. A typical reservoir landslide in the Three Gorges Reservoir area was selected as the case study. The change characteristics of underground water seepage were analyzed via the finite element method in a numerical model, and the influence of reservoir water fluctuation on the seepage field in the landslide was discussed. Combined with in situ monitoring data, the landslide deformation characteristics considering soil rheology properties were quantitatively examined, which is very important for research on similar reservoir landslides in the Three Gorges Reservoir area.

2. Materials and Methods

The Huangtupo landslide is located in Badong County, at a longitude of 110°22′58.48″ E and latitude of 31°2′33.73″ N, on the south side of the Yangtze River and 69 km away from the Three Gorges Dam site (Figure A1). The front edge of the landslide is approximately 80 m in elevation, and the base of the trailing edge is 650 m. The landslide covers an area of 1.35×10^4 m^2, with a mean longitudinal dimension of 1780 m and a width of 700 m. The mean depth of the sliding surface is approximately 30 m.

The Huangtupo landslide consists of four small subordinate landslides that occurred successively: Riverside Slump #1, Riverside Slump #2, Garden Spot Landslide, and Substation Landslide (Figure A1c). The Riverside Slump #1 and the Riverside Slump #2, with volumes of 22×10^6 m^3 and 20×10^6 m^3, respectively, are the first two landslides that started to fail and slide and have since been the principal part of the Huangtupo landslide. Then, the Substation Landslide, with a volume of 13×10^6 m^3, started to slide, with its front edge overlying Riverside Slump #1 and Riverside Slump #2, followed by the Garden Spot Landslide, with a volume of nearly 14×10^6 m^3 (Figure A2).

Presently, the Riverside Slump #1 is the most unstable, as its deformation is more obvious than that of the other landslides [16]. Therefore, the Riverside Slump #1 is chosen as the study object in this paper. The exposed bedrock strata of Riverside Slump #1 are mainly the Lower Triassic Jialingjiang Formation (T_{1j}), interlayered clastic strata and carbonate strata developed in the Middle Triassic Badong Formation (T_{2b}), consisting of limestone and dolomitic limestone, with a dip direction of 30° and a dip angle of 51° (Figure A3). Soil parameters of slip zone soil from Riverside Slump #1 were tested, as shown in Table A1. Figure A4 is a flowchart that illustrates the methodology used in this study.

2.1. Landslide Deformation

The failure mechanism of the Huangtupo landslide is characterized by a multistage evolution process [29]. The slope initially experienced a long-term downslope overlapping, including toppling and deep creeping. Later, the landslide was associated with some typical landforms, such as a terraced landscape, and displacement between the structural surface and the bedrock. Then, the landslide was continuously modified due to hydrologic and geomorphologic activities.

According to geological survey and monitoring data, a linked surface does not exist in the riverside accumulated mass. However, the displacement in the slip zone of Riverside Slump #1 is significant, and this landslide is currently in the creeping deformation state. Highly influenced by the dynamic seepage of underground water generated from rainfall and regular water level fluctuation, the deformation of Riverside Slump #1 is increasing significantly and will reach the criterion state of failure if it is not controlled artificially.

2.2. Ground Surface Monitoring

A comprehensive and spatial multiphase monitoring system has been installed on the Huangtupo landslide by China University of Geosciences (Wuhan) to monitor its ground surface deformation, deep deformation, underground water level, etc. There are 9 GPS monitoring points distributed on the Riverside Slump #1 to monitor its ground surface deformation, as shown in Figure A5.

The cumulative displacement and deformation rate of each monitoring point is shown in Figure A6. Generally, the cumulative displacement of the frontal part varies between 153.08 mm (G1) and 190.09 (G20) mm; the cumulative displacement of the central part is approximately 250.71 mm, 193.46 mm, 110.90 mm, and 182.01 mm at G7, G9, G18, and G22, respectively; the cumulative displacement of the upper part is 71.1 mm. The deformation rates show a significant difference in space, and the frontal part has the largest deformation rate at 2.57 mm/month, followed by the central part at 2.05 mm/month and the upper part at 0.64 mm/month. Additionally, the deformation rates in the same areas are found to be very similar.

According to the analysis of monitoring data, the Riverside Slump #1 is currently in the creep deformation stage, and the deformation is growing with time and closely related to the fluctuation of water level. The influence of water level fluctuation weakens as the distance from the Yangtze River increases.

2.3. Numerical Simulation Model

The finite element method based on unsaturated-unsteady seepage theory is adopted in simulating the seepage field of landslides with respect to fluctuations in reservoir water levels. The principal of mass conservation is available for both saturated and unsaturated condition [30], according to Darcy's law and the law of conservation of mass, the two-dimensional differential equation of seepage can be deduced as written in Equation (1), wherein piezometric head (h) is the variable.

$$\frac{\partial}{\partial x}\left(k_x\frac{\partial h}{\partial x}\right)+\frac{\partial}{\partial y}\left(k_y\frac{\partial h}{\partial y}\right)+Q=m_w\gamma_w\frac{\partial h}{\partial t} \quad (1)$$

Herein, k_x and k_y are the horizontal and vertical saturation permeability coefficients, respectively; h is the total piezometric head; Q is the boundary flow quantity; m_w is the water capacity; and γ_w is the water unit weight.

The model is built based on section line I-I′ (Figure A7), with dimensions of 940 m in the horizontal direction and 357 m in the vertical direction. The model consists of six parts: Upper slip mass, upper slip zone, lower slip mass, lower slip zone, rear deposit mass, and bed rock. The physical mechanical parameters of each zone used in the numerical simulation are shown in Table A2.

Previous studies have indicated that there are two main factors controlling the seepage field in landslides: The reservoir water level and the rheological properties of the geotechnical material.

According to the in situ monitoring data, the annual fluctuation process of the reservoir water level is divided into four stages, as follows:

Stage 1 water level rises from 145 m to 175 m in 30 days with a rate of 1.0 m/d.
Stage 2 water level is sustained at 175 m for 60 days.
Stage 3 water level declines slowly from 175 m to 145 m in 150 days at 0.2 m/d.
Stage 4 water level is sustained at 145 m in the following 120 days.

The relation between water level and time can be generalized in Equation (2).

$$\mathrm{H}(t) = \begin{cases} 145 + t, \ t \in [0,\ 30\mathrm{d}] \\ 175, \ t \in (30,\ 90\mathrm{d}] \\ 175 - 0.2(t - 90), \ t \in (90,\ 240\mathrm{d}] \\ 145, \ t \in (240,\ 360\mathrm{d}] \end{cases} \tag{2}$$

Herein, the unit of t is d. The seepage field in the landslide is mainly influenced by the infiltration coefficient of the geomaterial, the fluctuation rate of the reservoir water level, and the thickness of the aquifer; the infiltration coefficient is the most critical factor for a given landslide when the other two factors are fixed. The hydraulic conductivity of geomaterial in modeling is estimated using the Fredlund and Xing model in Geostudio SEEP/W, and the relation between volumetric water content θ and matric suction φ is expressed in Equations (3) and (4).

$$\frac{\theta}{\theta_s} = F_{(\varphi)} = C_{(\varphi)} \frac{1}{\left\{\ln\left[e + (\varphi/a)^b\right]\right\}^c} \tag{3}$$

$$C_{(\varphi)} = 1 - \frac{\ln(1 + \varphi/\varphi_r)}{\ln\left(1 + 10^6/\varphi_r\right)} \tag{4}$$

Herein, a, b, c are fitting parameters related to the air entry value of the soil; θ_s is the saturated volumetric water content; and φ_r is the corresponding matric suction at residual water content. $\theta \in [0, \theta_s]$, $\varphi \in [0, \varphi_{max}]$, and φ_{max} are the maximum matric suction when the water content is zero.

The dynamic water head is assigned to the right boundary in the model according to the fluctuation of reservoir water level, and the constant water head at the left boundary is 210 m, as indicated by the in situ monitoring data. The initial seepage field is first simulated by setting the water head of the right boundary to 145 m; then, the dynamic change in the seepage line during the annual fluctuation of the reservoir water level can be analyzed.

3. Results

3.1. Seepage Line Analysis

To reveal the change in the seepage line when the reservoir water level fluctuates between 145 m and 175 m annually, the interval water level is set to 5 m. During the impoundment and drawdown of reservoir water, the seepage line is exported from Geostudio SEEP/W when the water level is 145, 150, 155, 160, 165, 170, and 175 m, as illustrated in Figure A8.

During the period when the reservoir water level rises from 145 m to 175 m, the seepage line in the slip mass gradually increases and morphologically transforms from a straight line to a concave line that inclines to the slope. During the initial increase in the reservoir water level from 145 m to 150 m, the seepage line is more like a straight line parallel to the horizontal direction, and the supply of reservoir water to underground water is mainly concentrated at the deep level of the landslide. Afterwards, the seepage line turns to a concave shape and nearly 90° to the horizontal direction, and the supply of the reservoir water is transferred to the shallow level of the landslide. Meanwhile, the water head between the reservoir water and the underground water increases persistently at this

stage, as well as the penetration water pressure directed to the landslide; hence, the stability of the landslide will be improved by increasing the reservoir water level.

During the early decline of the reservoir water level, the angle between the seepage line and the horizontal direction is approximately 20°. At this stage, the penetration effect of underground water is not evident, and the effect of the reservoir water on the landslide is reflected by the generation of hydrostatic pressure. As the reservoir water declines continuously, the angle between the seepage line and the horizontal direction decreases to nearly 5°. This result means that the incline of the seepage line is gentle and that the underground water discharge is dominated by horizontal drainage. The water head between the underground water and the reservoir water causes the discharge of underground water to substantially penetrate the landslide, thus improving the sliding force of the slide body. The fall of the reservoir water level is a disadvantage for slope stability.

Generally, changes in the seepage line lag behind changes in the reservoir water level. This finding can be explained by the low permeability of geotechnical material, which is far smaller than the rise rate and fall rate of the reservoir water. The rise in the reservoir water level provides an inward replenishment for the underground water seepage in the landslide, and the seepage line is mainly a concave shape and inclines to a slope. When the underground water creates an outward discharge to the reservoir water during the fall of the reservoir water level, the seepage line is characterized by a convex shape and inclines to the Yangtze River.

3.2. Deformation Characteristics

The rheological effect of slip zone soil on landslide deformation is discussed through numerical modeling in the finite differential software FLAC3D, which is widely used in geological engineering owing to its advantages in simulating plastic flow, yield, softening, and even large deformation of material. The rheological property of the slip zone was studied [31], and the H-K constitutive model was adopted to describe the rheological behavior in this research, as written in Equation (5).

$$\varepsilon_{(t)} = \frac{\sigma_0}{E_0} + \frac{\sigma_0}{E_1} - \frac{\sigma_0}{E_1} e^{-\frac{E_1}{\eta} t} \tag{5}$$

Herein, σ_0 is the constant stress; E_0, E_1 is the elastic modulus related to the instantaneous strain and linear strain, respectively; η is the viscosity coefficient related to the attenuation creep. According to the experimental result [31], $\sigma_0 = 0.5$ kPa, $E_0 = 14.19$ kPa, $E_1 = 37.51$ kPa, $\eta = 948.90$ kPa $\cdot$ h.

The influence of the change in reservoir water level on landslide deformation is taken into consideration by exporting seepage results into the model from Geostudio SEEP/W. To reduce the calculation time during numerical modeling, the water table at every 5 m of reservoir water level fluctuation is extracted and imported to FLAC3D for numerical modeling. The initial stress equilibrium is first achieved when the water level reaches 145 m.

According to the displacement-time curves in Figure A9, the investigated landslide is characterized by creep and step-like deformation. Deformation of M1~M4 develops in the same tendency, and the total displacements over the whole year are 46.05, 17.47, 13.45, and 9.38 mm, respectively.

3.2.1. Impoundment

It should be noted that deformation of M1 remarkably rebounds during the rise of the reservoir water level, as shown in Figure A10. The reason for this rebound could be the point located at the frontal part of the landslide; the rise in water level increases the normal stress on the ground surface and, consequently, the resistance force against sliding. As the reservoir water level increases at a speed of 1 m/d in the numerical model, the change in the seepage line lags behind the change in the water level, which is why rebound deformation is observed from five days when the water level rises to 150 m. Afterwards, with the completion of pore water pressure adjustment, deformation starts to increase continually from 20 days. The total rebound deformation is estimated to be 2.66 mm, and the

final deformation of M1 caused by the rise in water level is 1.7 mm, accounting for 3.7% of the total annual deformation.

The positive influence of the rise in the reservoir water level on landslide stability is mainly focused on the frontal and central parts of upper slip mass, reflected by the obvious rebound on the displacement-time curves of M1 and M2. Simultaneously, deformation continues to increase slowly at the upper part of both the upper slip mass and the lower slip mass.

3.2.2. Drawdown

The deformation behavior in a short period (25 days) is investigated first via numerical modeling. The displacement contour of the investigated landslide when the reservoir water level decreases from 175 m to 170 m is shown in Figure A11, and the evolution process of deformation can be divided into four stages:

(1) When the reservoir water level starts to fall, an instantaneous elasto-plasticity deformation is generated at the upper shear outlet of the landslide due to the unloading effect caused by the fall in the reservoir water level. Deformation in this stage is observed only at the shear outlet of the landslide and is as small as 0.01 mm, as shown in Figure A11a.

(2) Afterwards, deformation slightly increases under the effect of stress adjustment in the landslide. In the next 0.5 days, the combined effect of hydrodynamic pressure and reservoir water unloading leads to additional stress in the landslide, and this additional stress accelerates the landslide deformation. The predominant deformation still occurs in the slip mass, while the deformed zone extends downward to the nearby phreatic line. Compared to the displacement in the first stage, in this stage, it is small at approximately 0.7 mm, as shown in Figure A11b.

(3) As the water level continuously falls, the additional stress slowly transmits to the slip zone, and creep deformation is observed in the slip zone. From 0.5 to 1.5 days, the overall deformation of the landslide in this stage is mainly controlled by the slip zone, and creep deformation gradually develops to the ground surface. There is a significant increase in deformation at this stage, and the maximum displacement is approximately 4.46 m, as indicated in Figure A11c.

(4) In the following deformation stage, stress adjustment in the landslide is almost completed after 1.5 days. The overall deformation of the landslide develops at a constant speed under the rheological effect of the slip zone soil, as shown in Figure A11d.

The deformation at 4 (M1~M4) different locations is recorded in numerical modeling calculations, as shown in Figure A7. The horizontal distance between these monitoring points and the Yangtze River is 315, 405, 560, and 800 m, respectively. The corresponding displacement curves are plotted in Figure A12.

The deformation shows distinct spatial differences according to the time-displacement curves, as follows:

(1) The total displacement of each point is 6.06, 4.08, 4.75, and 4.31 mm, corresponding to M1, M2, M3, and M4, respectively. Greater deformation can be observed closer to the shear outlet of the landslide.

(2) The startup time of creep deformation and creep rate varies in space. For monitoring points M1~M4, the startup time of creep deformation is 0.4, 0.2, 0.1, and 0.08 d, respectively, as shown in Figure A12a. Since shear stress is mainly concentrated at the shear outlet of the landslide where soil suffers high deviatoric stress, the creep rate is relatively higher as it approaches the shear outlet. The steady creep speed of each monitoring point is 0.24, 0.16, 0.18, and 0.17 mm/d, corresponding to M1, M2, M3, and M4, respectively.

(3) The displacement at the slip zone is smaller than that at the ground surface, and there is a remarkable jump at the depth of the upper slip zone, as shown in Figure A12b in the deformation curve. In the creep deformation stage, the overall deformation of the landslide is mainly controlled by the slip zone, so there is only a small variation in the overlying slide mass.

Based on the short-term deformation characteristics, further analysis on the long-term deformation characteristics during the decline in the reservoir water level is carried out, and the time-displacement curves are plotted in Figure A13.

(1) As the reservoir water level decreases, the hydrodynamic pressure continues to increase. However, the increment of hydrodynamic pressure reduces in the meantime, leading to deformation developing at a deceasing creep speed. Therefore, the deformation curve of each monitoring point shows attenuation characteristics.

(2) In the steady creep stage, the creep rate also has obvious spatial variability, similar to that of the short-term deformation characteristics, namely, higher creep speeds are found closer to the shear outlet of the landslide. The creep speeds are 0.29, 0.087, 0.071 and 0.054 mm/d in descending order corresponding to M1~M4. The total displacement of M1~M4 during the decline in the reservoir water level is 43.56, 13.05, 10.69 and 8.12 mm, respectively.

(3) By comparing the results of numerical modeling with in situ monitoring data, the displacement is found to be consistent at the same order of magnitude. The displacement rates of M1, M2, and M4 are compared with those of G2, G7, and G18 in practice (from January to June 2007), and the mean bias between them is approximately 3.4%, 5.1%, and 0.6%, respectively. Although the deformation rate calculated from numerical modeling is consistent with that obtained from in situ monitoring, the bias between the displacement values is distinctively large. This finding occurs because some preventive treatments were carried out at the toe of the landslide, thus slowing deformation and improving landslide stability. However, the deformation characteristics are reliable, and the results can be used for further analysis.

(4) Since it takes a long time for the adjustment of seepage field and stress during the drawdown of reservoir water level, landslide deformation usually lags behind the change in reservoir water level, and the hysteresis time is approximately 30 days according to in situ monitoring data. As the underground water table in numerical modeling is imported from the computation result of the previous simulation, the stress adjustment time is thus shortened to 0.5 days.

The ultimate deformation of M1~M4 generated during the decline in the water level is 43.56, 13.05, 10.69, and 8.12 mm, contributing to 94.59%, 74.70%, 79.48%, and 86.57% of the total deformation, respectively. The deformation of the landslide is severe when the water level decreases from 175 m to 145 m.

The steady creep deformation rates of M1~M4 are 0.19, 0.072, 0.056, and 0.039 mm/d when the reservoir water level is settled at 145 m, smaller than that during the declining stage of the reservoir water level. This result also indicates that the frontal part of the upper slip mass is more sensitive to fluctuations in the reservoir water level, which is also proven by previous analyses.

3.3. Deformation Mechanism

Based on previous deformation analysis, it is known that the investigated landslide is in the creeping deformation stage and is highly influenced by the fluctuation of the reservoir water level. Figures A14 and A15 are the displacement contours obtained in numerical simulation. The deformation mechanism is analyzed as follows, with respect to the fluctuation of the reservoir water level.

(1) After the initial stress equilibrium is completed, the reservoir water level quickly rises at a speed of 1 m/d and causes uplift pressure at the toe of the landslide until the water level reaches 150 m. In addition, the mechanical strength of the geomaterial in this area is softened by water saturation. The combined effect of uplift pressure and water softening reduces the weight of the slip mass at the toe of the landslide, thus lowering its sliding resistance force. Thus, deformation in this stage is mainly observed at the upper part and central part of the landslide and develops in the sliding direction.

(2) With the sustaining rise in the reservoir water level, the slide body suffers the hydrostatic pressure generated by the pressure difference between the reservoir water level and the underground

water table of the slide body, which improves the sliding resistance force and leads to an obvious deformation rebound at the frontal part and central part of the slip mass. Landslide deformation in this stage develops slowly at the upper part of the slip mass, but the overall stability is improved.

(3) When the reservoir water level rises to 170 m, the pore water pressure adjustment is almost complete, and deformation is observed near the upper shear outlet of the landslide. Afterwards, deformation develops from the upper part to the frontal part and as the reservoir water level increases to 175 m.

(4) During the declining stage of the reservoir water level, the largest deformation is still concentrated near the upper shear outlet and increases to 57.3 mm when the water level decreases to 145 m. The investigated landslide is characterized by a retrogressive landslide, and the deformation mechanism is closely related to the fluctuation in the reservoir water level.

Generally, the shear strain increment in the drawdown stage of the reservoir water level is larger than that in the impoundment stage. The maximum shear strain increment is indicated to be 6.6 when the reservoir water level declines to 145 m.

4. Discussion

The failure criterion and the reduced strength are the key factors in the application of the shear strength reduction method for slope stability analysis [32]. The overall failure criteria for soils on a slope can be divided into three types: Nonconvergent iterations of static equilibrium in finite element numerical solutions, a plastic zone (or equivalent plastic strain) along the full slope from the toe to the top, and a sudden and continuous change in the strain and displacement of the sliding surface. However, it is hard to take nonconvergent iterations as the failure criteria when the rheological property was taken into account in the calculation, which can be explained by the fact that the maximum unbalance force is not infinitely small in every time step as it used to be in strength reduction analysis. In addition, a plastic zone along the full slope does not mean that an overall collapse occurred, while sudden nodal displacement changes at a certain point means that no stress distribution can be achieved to satisfy both the yield criterion and global equilibrium. Therefore, a sudden change in the displacement–time curve is chosen as the failure criterion in this research.

Based on the previous analysis, the influence of underground seepage and rheological properties are both taken into account to explore the evolution of landslide stability. The entire deformation process is shown in Figure A16. The displacement–time curve indicates that deformation before failure is characterized by attenuation of the creep stage and steady creep stage, while the time when deformation enters into the acceleration creep stage is almost the same in space. The evolution process of the acceleration creep stage is consistent among these locations and can be divided into three substages:

(1) Slow acceleration creep stage. During the decline in the reservoir water level, the creep deformation increases slowly at a constant creep acceleration, reflected by the linear creep rate in Figure A17. For every 5 m decline in the reservoir water level, the increase in the creep rates of M1~M4 are 0.051, 0.024, 0.021, and 0.017 mm/d, respectively.

(2) Fast acceleration creep stage. With the continuous drawdown of the reservoir water level, the creep acceleration increases in a nonlinear relationship with time, as well as the creep rate. The ultimate increase in creep rate in this stage for M1~M4 is approximately 0.161, 0.125, 0.055, and 0.017 mm/d, respectively.

(3) Rapid acceleration creep stage. As indicated by Figure A17, a noteworthy inflection point is observed at the displacement–time curve, which means that the investigated landslide begins to fail at this moment. The frontal part starts to fail first, followed by the central part and upper part almost simultaneously. The creep rates of M1~M4 at this stage are approximately 0.478, 0.185, 0.078, and 0.016 mm/d, respectively.

The monitoring data collected from September 2004 to August 2010 are used to compare with numerical simulation results as shown by Figure A18. The cumulative displacement of G2, G7, and G18 in the six years is 155 mm, 152.68 mm, and 71.82 mm, respectively. The numerical results show that the cumulative displacement is 100.21 mm, 43.62 mm, and 36.70 mm corresponding to M1, M2, and M4. It can be noted that deformation from in situ monitoring and simulation seems inconsistent in magnitude, the reason behind this being that the material parameters used in the modelling are homogeneous, which were tested by limited number of soil samples, that may not agree with practical situation. Moreover, some complicated geological factors were ignored or generalized in modeling, as well as the nature environment and the human activities. However, the deformation rate calculated from numerical modelling is consistent with that obtained from in situ monitoring, which means the response regularity of landslide deformation to the water level fluctuation is the same, and the reliability of deformation mechanism obtained from simulation results can be confirmed.

5. Conclusions

In this study, the underground seepage characteristics in the landslide were discussed by numerical modeling in Geostudio SEEP/W, and the rheological properties of the slip zone were taken into consideration in the study of the long-term deformation of the Huangtupo landslide. The following conclusions have been made:

(1) Generally, the change in seepage lines always lags behind the fluctuation of the reservoir water level due to the low permeability of the geotechnical material. When the reservoir water level rises, the underground water seepage is replenished in the landslide, and the seepage line is mainly in a concave shape and inclines to a slope. While the underground water creates an outward discharge to the reservoir water when the reservoir water level declines, the seepage line is characterized by a convex shape and inclines to the Yangtze River.

(2) The evolution process of the investigated landslide is characterized by four stages, an instantaneous elasto-plasticity deformation generated at the shear outlet of the landslide due to the unloading effect caused by the decline in the reservoir water level. Then, stress adjustment occurs in the landslide, resulting in predominant deformation in the slip mass. As the reservoir water level continuously declines, the overall deformation of the landslide is mainly controlled by the slip zone, and creep deformation gradually develops from the slip zone to the ground surface. Finally, deformation develops at a constant speed under the rheological effect of slip zone soil after the completion of stress adjustment.

(3) In practical terms, it takes a long time for the seepage field and stress to adjust during the decline in the reservoir water level. Landslide deformation usually lags behind the change in reservoir water level, and the hysteresis time is approximately 30 days according to in situ monitoring data. This result occurs because the underground water table in numerical modeling is imported from the computation result of the previous simulation, and the stress adjustment time is thus shortened to 0.5 days.

(4) The investigated landslide is characterized by a retrogressive landslide, of which the deformation mechanism is closely related to the fluctuation of the reservoir water level. There is an obvious deformation rebound at the frontal part and middle of the slip mass during the rising stage of the reservoir water level. The sudden change in the displacement-time curve is selected as the failure criterion for the investigated landslide. The evolution process of the acceleration creep stage is divided into slow acceleration, fast acceleration, and rapid acceleration creep stages.

Author Contributions: Conceptualization, C.L.; methodology, C.L. and Y.W.; software, C.L. and Y.W.; validation, C.L. and H.T.; formal analysis, C.L.; investigation, C.L.; resources, H.T.; data curation, Y.W.; writing—original draft preparation, C.L.; writing—review and editing, C.L.; visualization, Y.W.; supervision, H.T.; project administration, H.T.; funding acquisition, H.T. All authors have read and agreed to the published version of the manuscript.

Funding: This research was funded by the Fundamental Research Funds for the Provincial Universities of Zhejiang (No. 22016000319030) and the National Major Science and Technology Projects of China, grant number 2017YFC1501300.

Conflicts of Interest: The authors declare no conflict of interest.

Appendix A

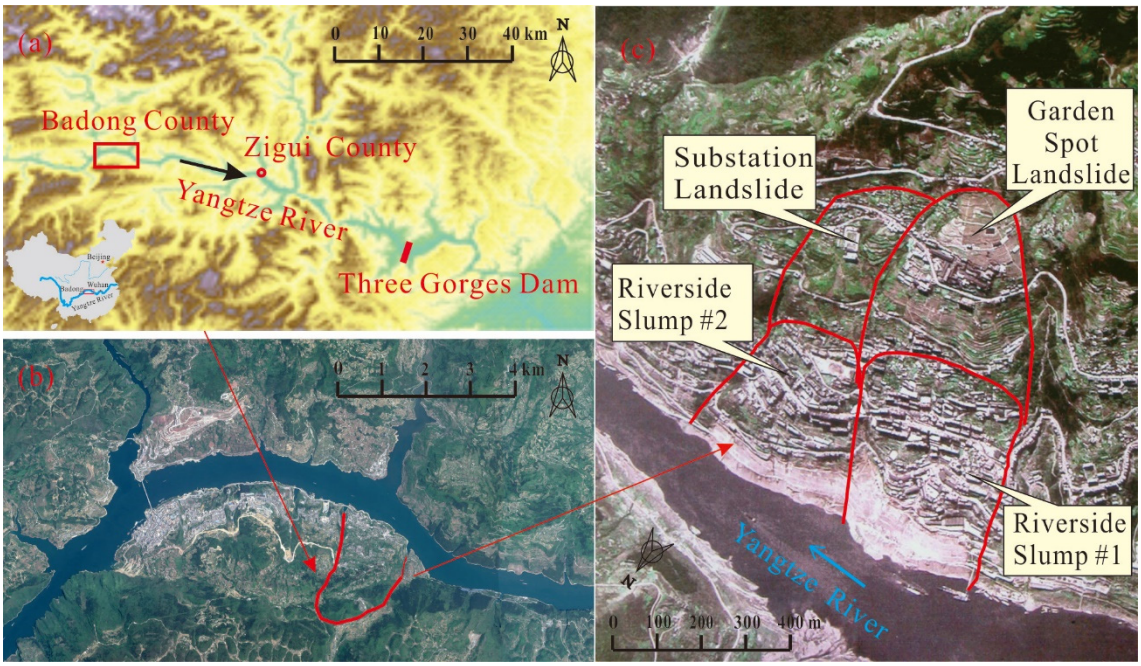

Figure A1. (**a**), (**b**) Satellite images showing the location of the study site in the Three Gorges Reservoir zone in central China; (**c**) Huangtupo landslide consists of four small subordinate landslides: Riverside Slump #1, Riverside Slump #2, Garden Spot Landslide, and Substation Landslide.

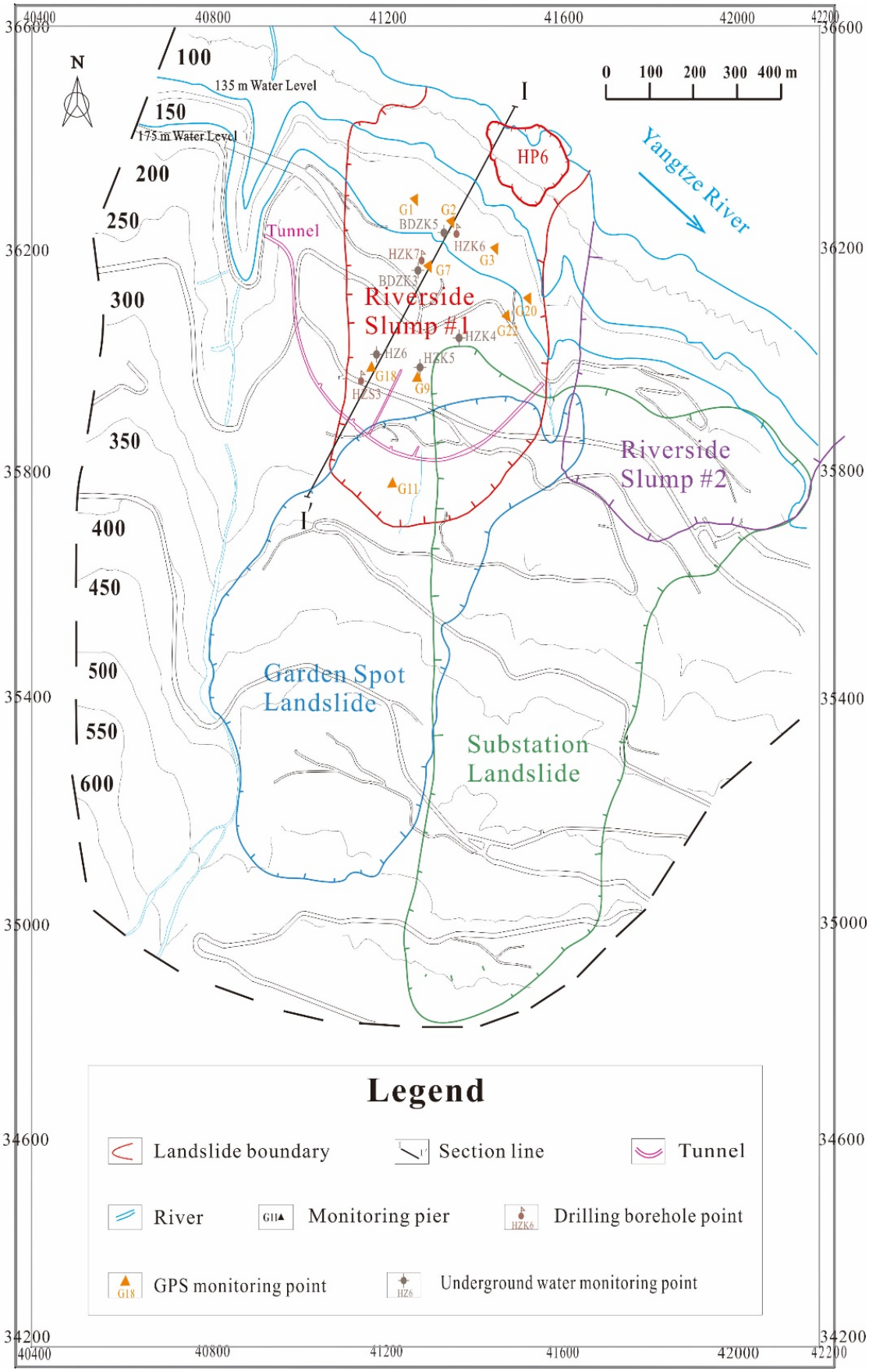

Figure A2. Engineering geological map of the Huangtupo landslide.

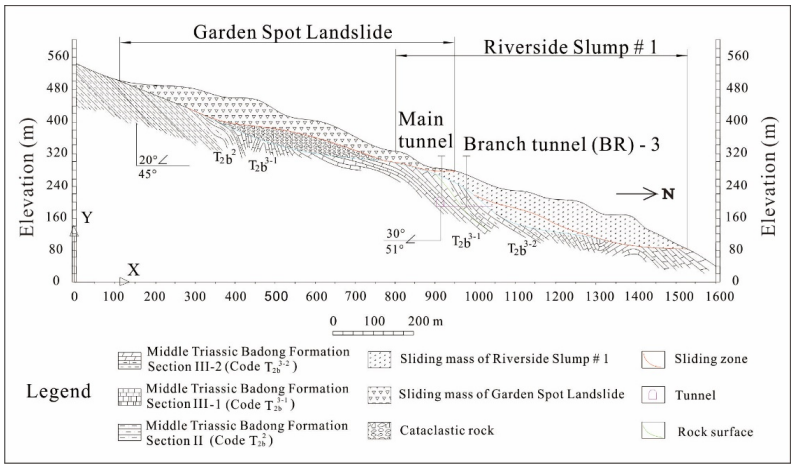

Figure A3. Engineering geological profile of the landslide along section line I-I′.

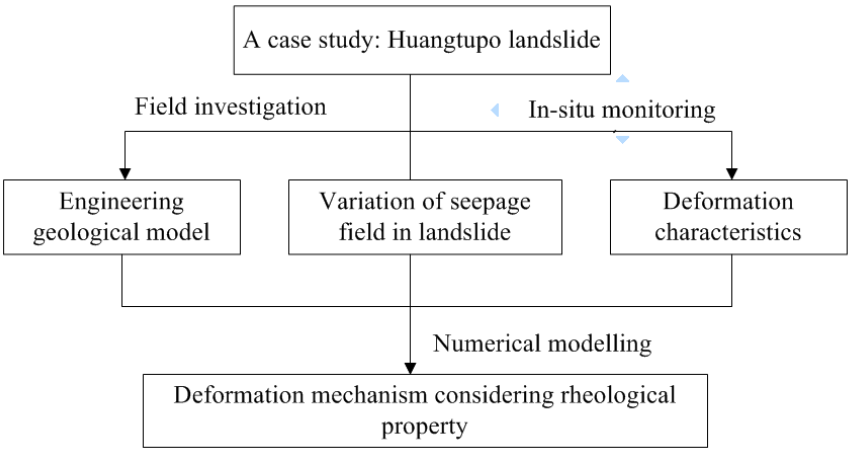

Figure A4. The methodology illustrated by a flowchart.

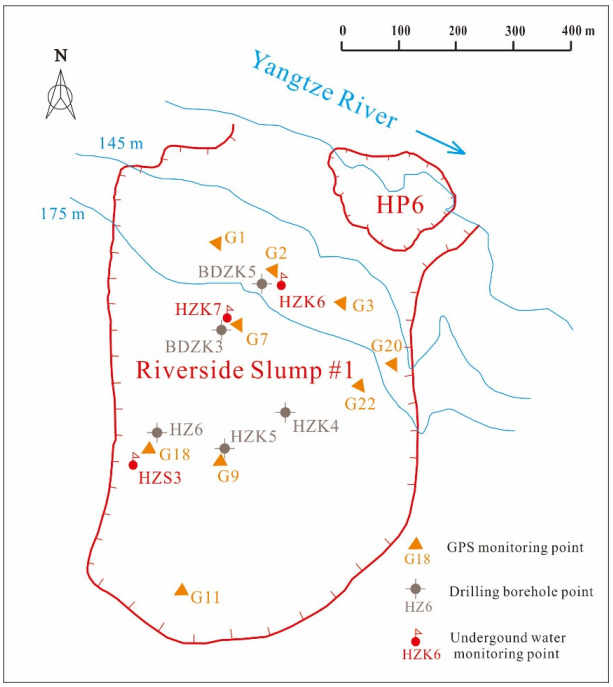

Figure A5. Monitoring points on Riverside Slump #1.

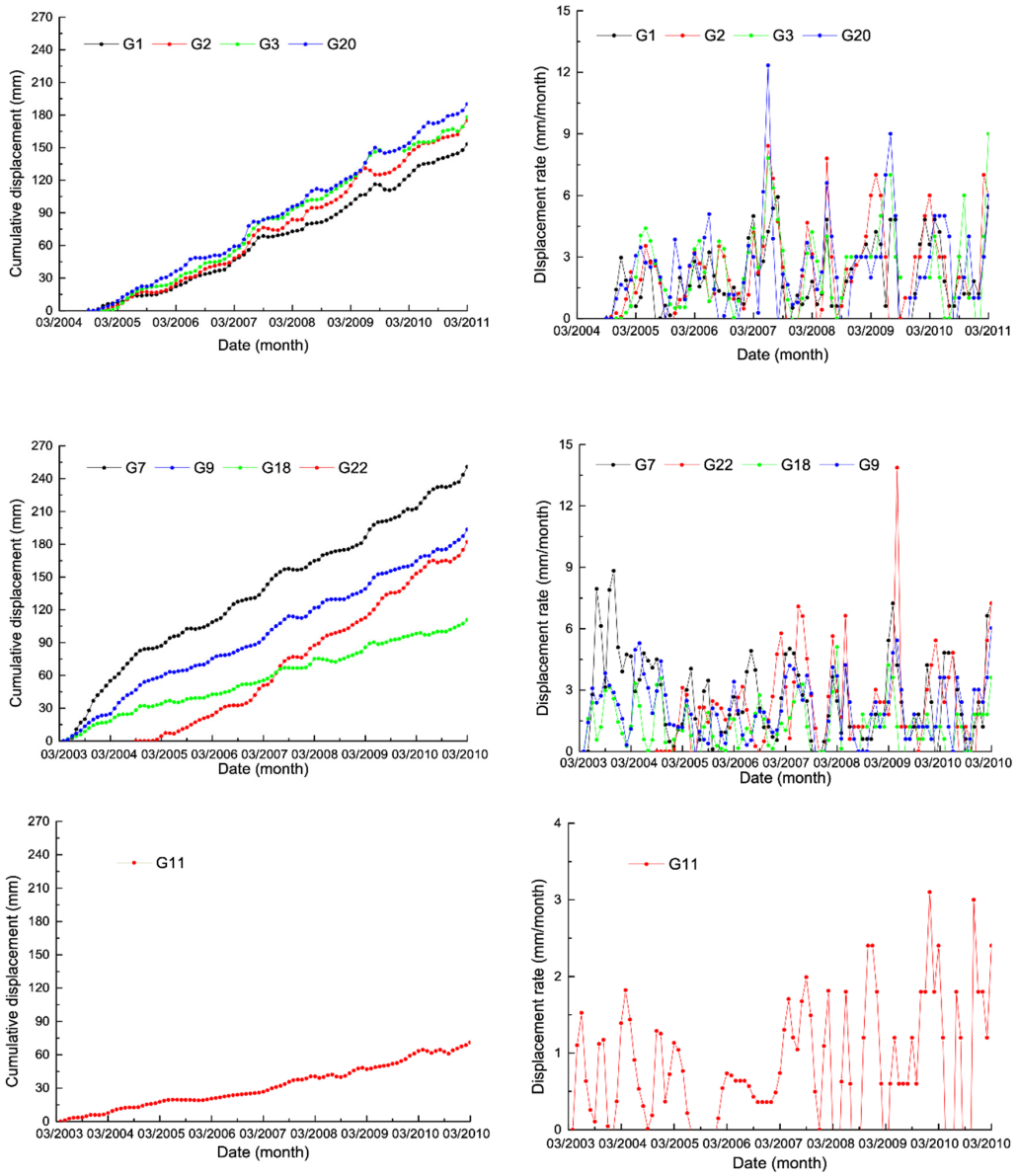

Figure A6. Cumulative displacements and displacement rates derived from GPS points.

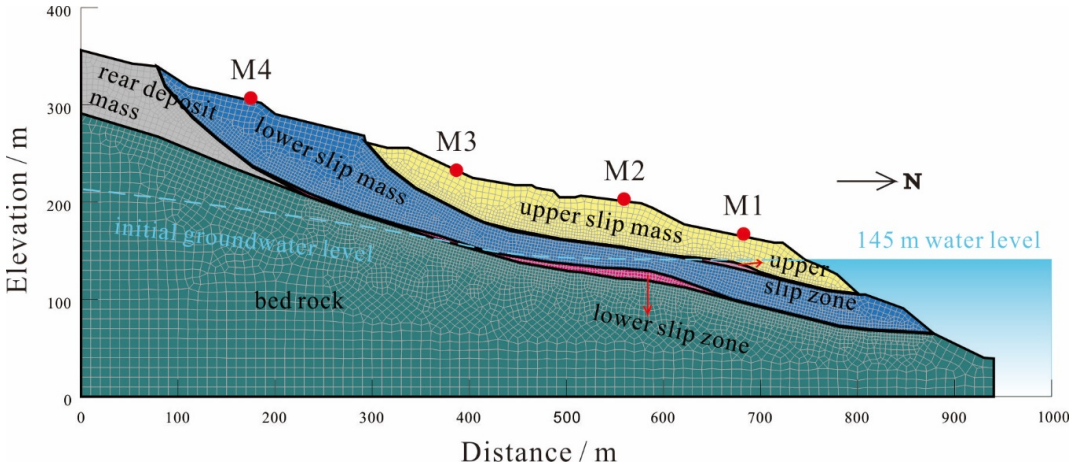

Figure A7. Simulation model of Huangtupo landslide.

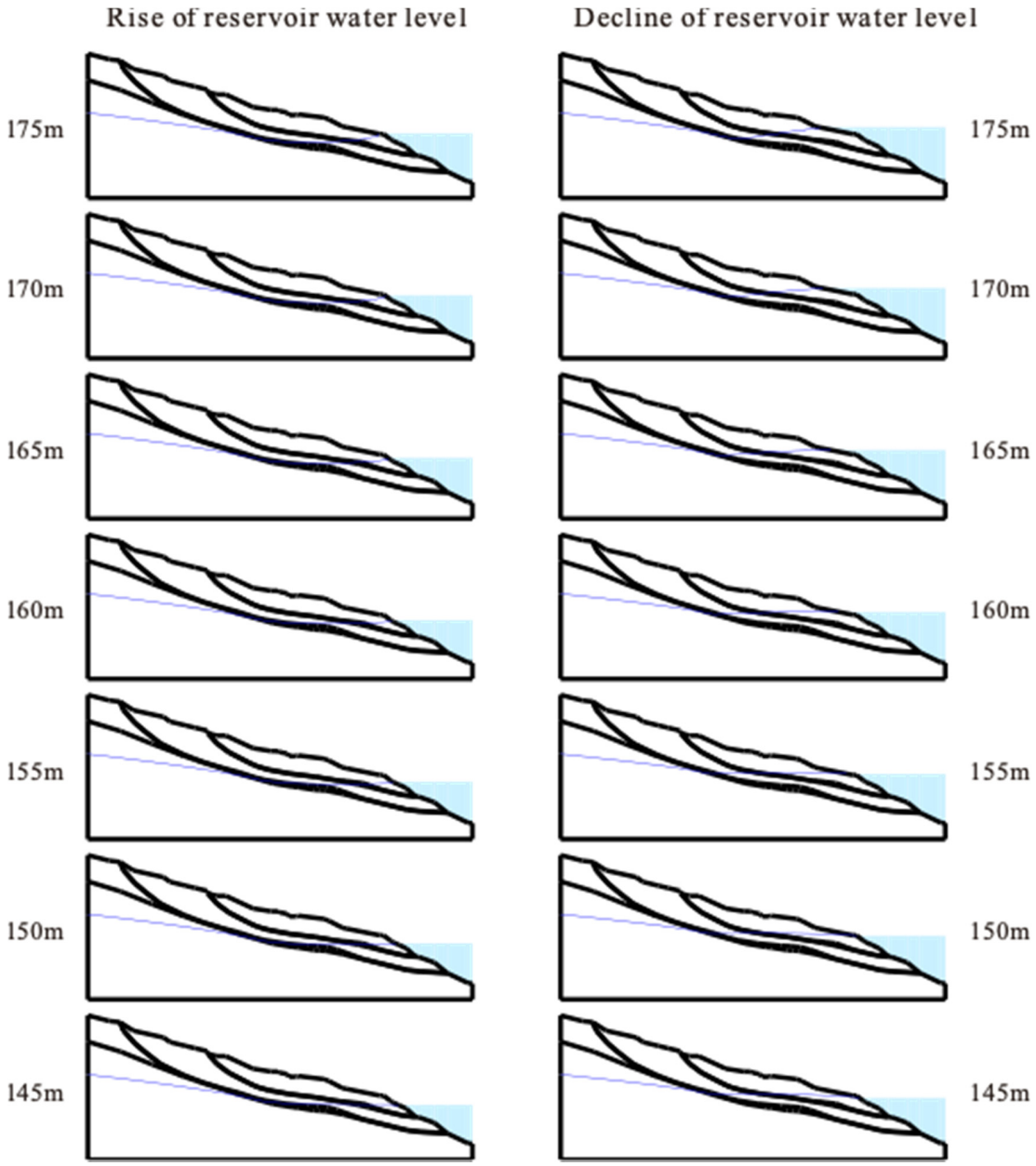

Figure A8. Change in seepage lines during the rise and decline in the reservoir water level.

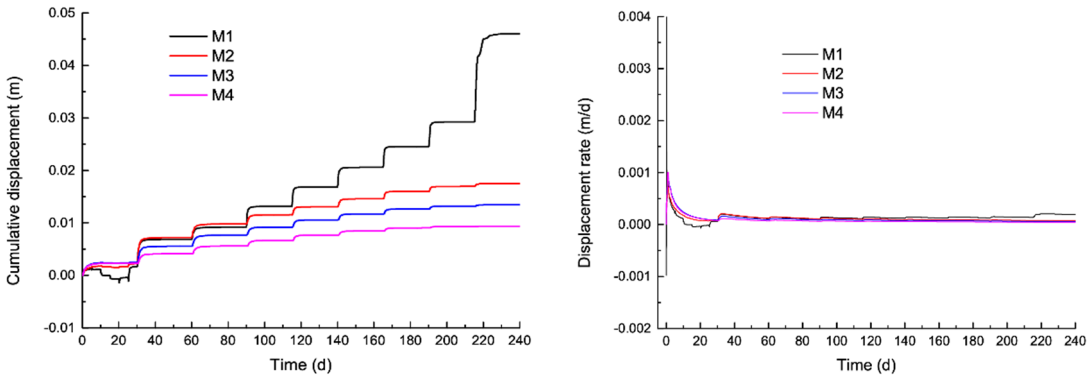

Figure A9. Surface displacement and displacement rate during the annual fluctuation of the reservoir water level.

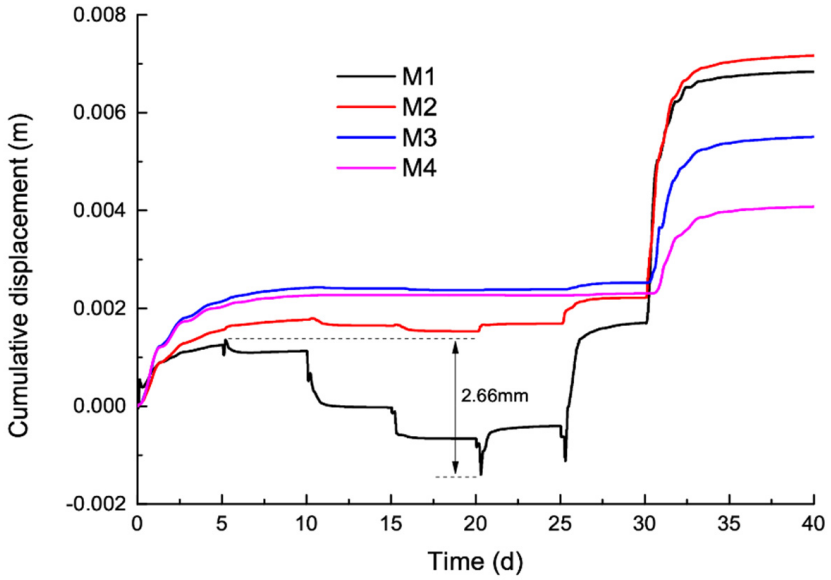

Figure A10. Surface displacement during the initial rise in the reservoir water level.

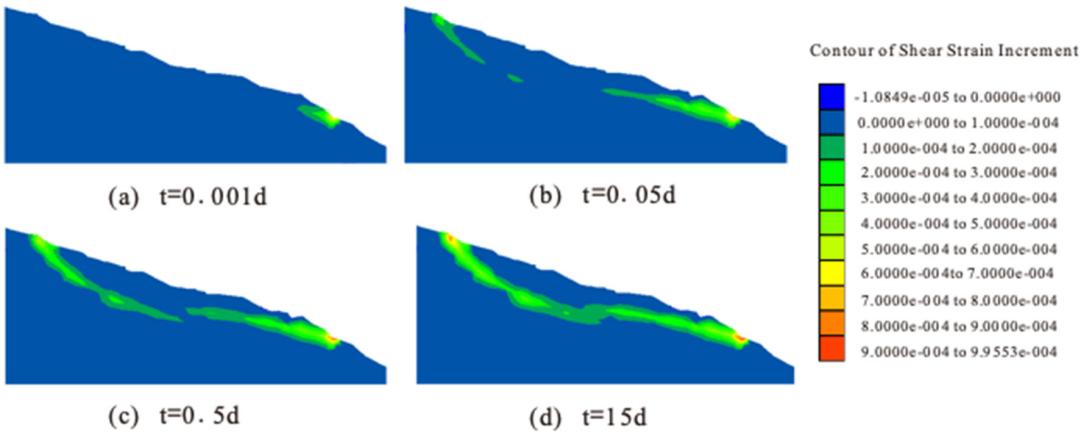

Figure A11. Contour of the shear strain increment during the decline in the reservoir water level.

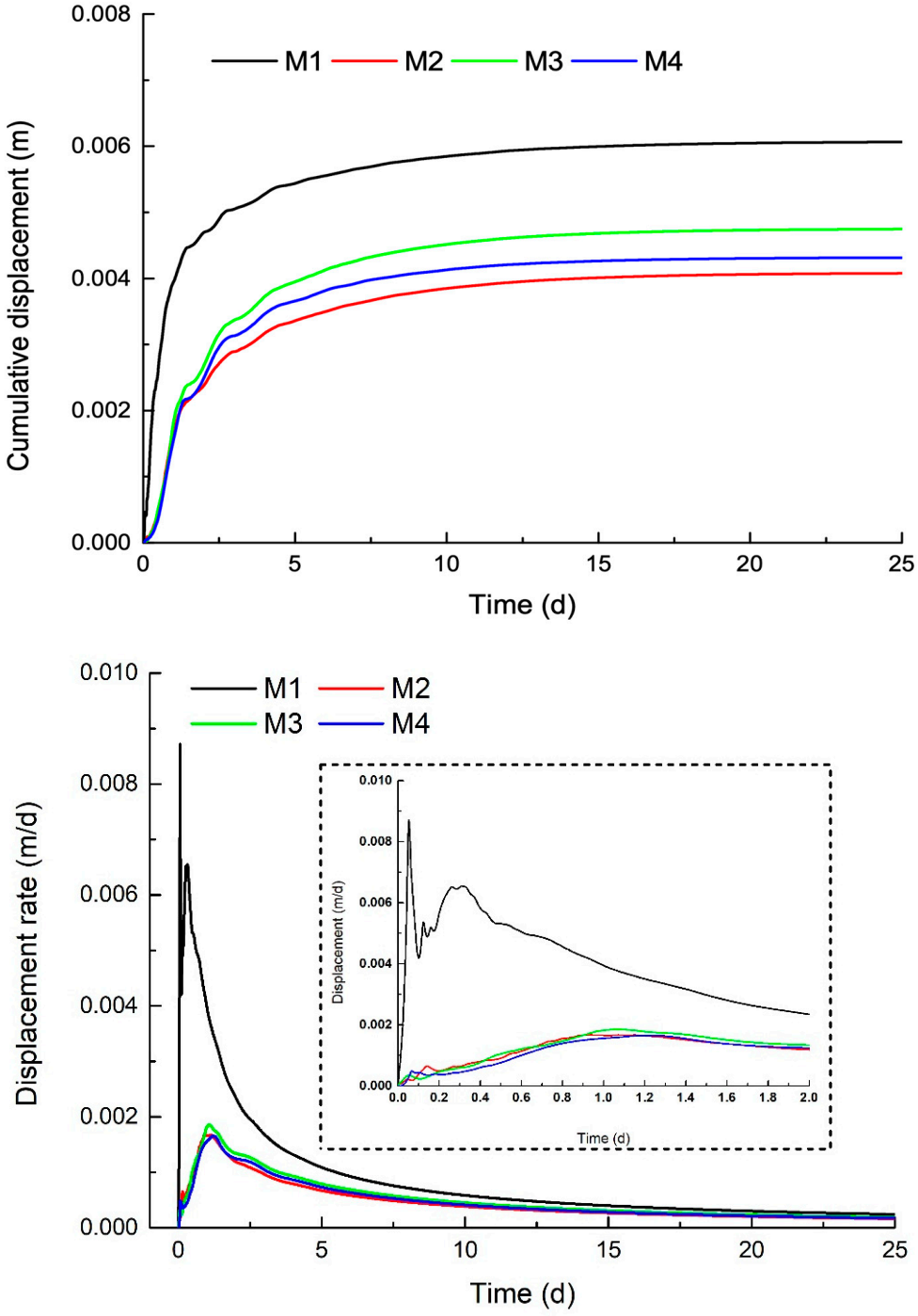

Figure A12. The simulated results: (**a**) The cumulative displacement of M1~M4; (**b**) The displacement rate of M1~M4.

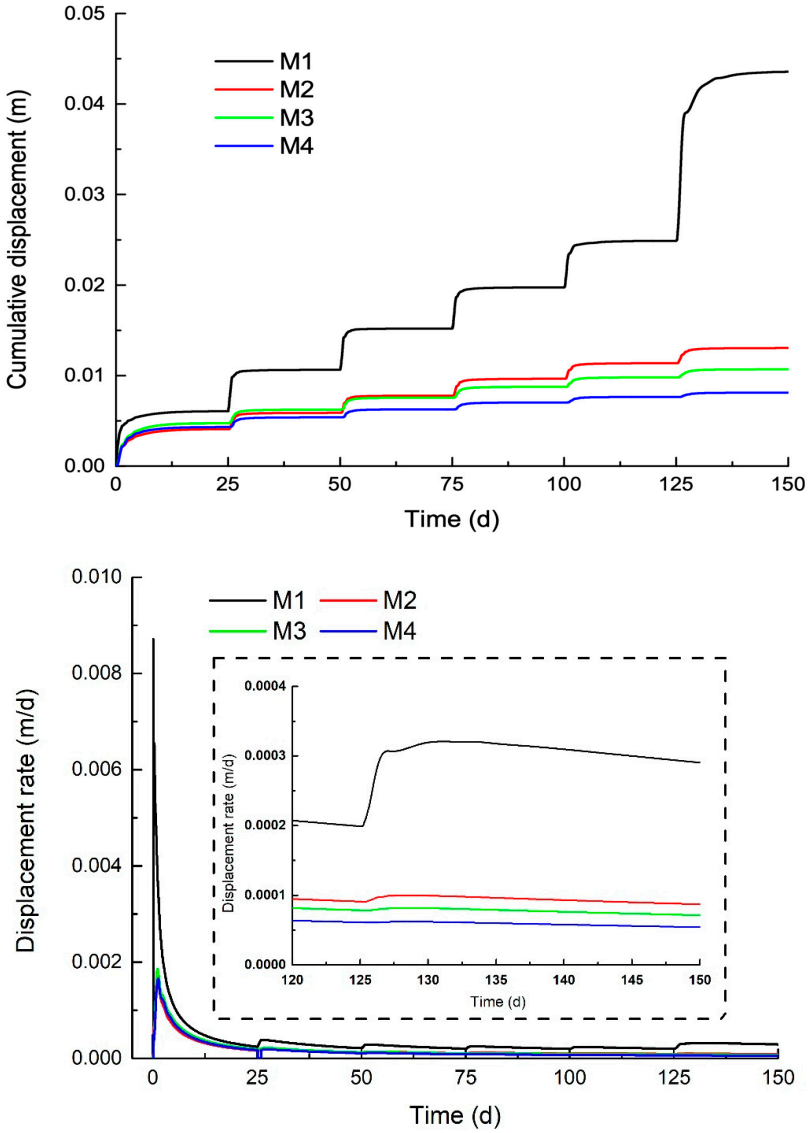

Figure A13. Surface displacement and displacement rate during the decline in the reservoir water level.

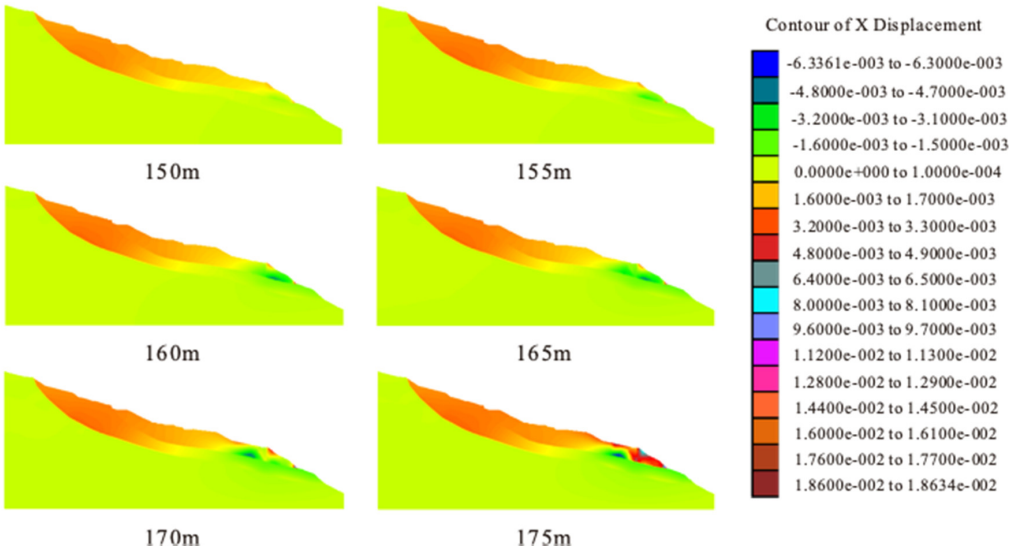

Figure A14. Contour of displacement during the rise in the reservoir water level.

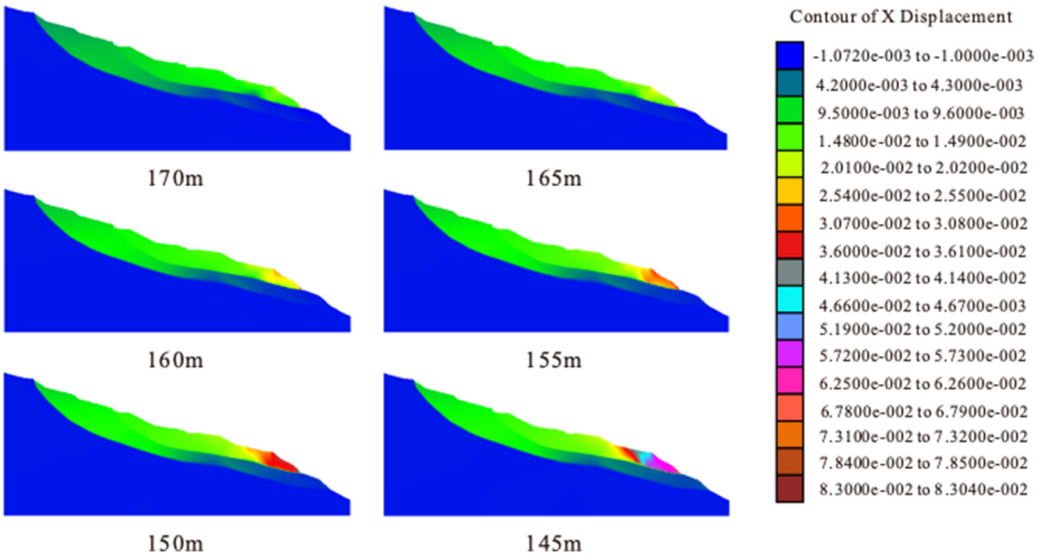

Figure A15. Contour of displacement during the decline in the reservoir water level.

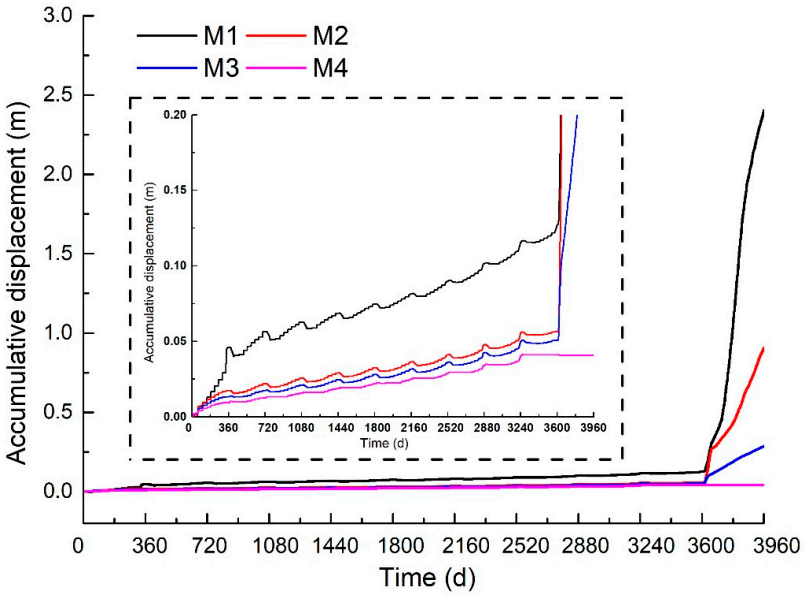

Figure A16. Entire deformation process.

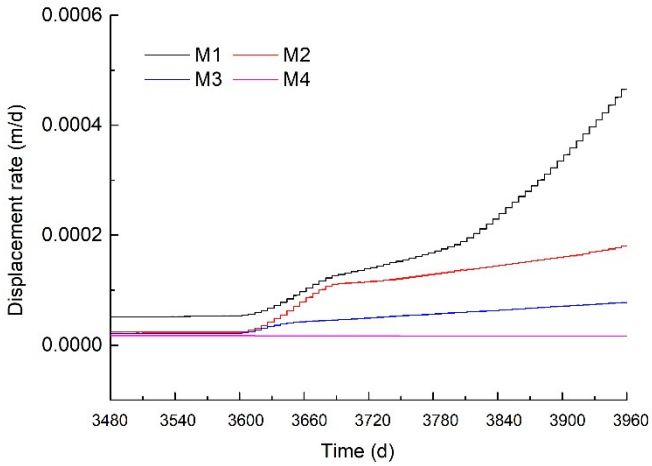

Figure A17. Creep rate in the 11th year.

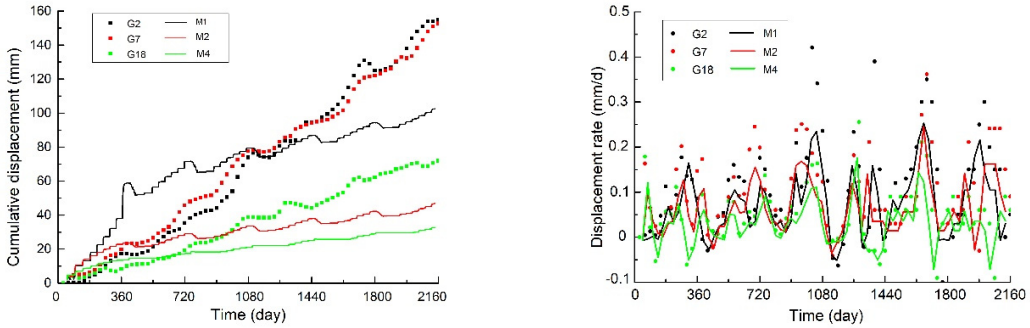

Figure A18. The comparison between monitoring and simulation (September 2004–August 2010).

Table A1. Physical properties of the slip zone soil.

Sets	Particle Size Fractions (%)				Liquid Limit (LL)	Plasticity Index (I_p)	Particle Density (ρ_s)	Water Content (w)	Dry Density (ρ_d)
	Gravel (>2 mm)	Sand (0.075~2 mm)	Silt (0.005~0.075 mm)	Clay (<0.005 mm)	%	/	g/cm^3	%	g/cm^3
HD-1	29.7	21.7	28.3	20.3	28.9	12.0	2.73	10.1	2.07
HD-2	35.9	19.2	26.5	18.4	28.2	11.5	2.73	9.7	2.07
HD-3	38.7	18.9	24.7	17.7	26.9	11.2	2.73	9.6	2.06
HD-4	39.1	13.1	28.5	19.3	28.4	11.9	2.73	9.9	2.07
Mean value	35.9	18.2	27.0	18.9	28.1	11.7	2.73	9.8	2.07

Table A2. Physical mechanical parameters used in the model.

Zone	Elasticity Modulus (MPa)	Poisson's Ratio	Unit Weight (kN/m^3)	Cohesion (kPa)	Friction Angle (°)	Saturated Infiltration Coefficient (m/d)	Porosity
Upper slip mass	727.0	0.31	21.0	80.0	25.0	2.35	0.392
Upper slip zone	28.6	0.34	19.9	33.0	16.0	0.76	0.318
Lower slip mass	2100.0	0.29	23.0	90.0	24.0	1.88	0.325
Lower slip zone	36.8	0.35	21.3	12.0	26.4	0.24	0.2925
Rear deposit mass	727.0	0.31	21.0	80.0	25.0	2.35	0.392
Bed rock	36,740.0	0.26	26.0	380.0	44.0	0.01	0.01

References

1. Muceku, Y.; Korini, O.; Kuriqi, A. Geotechnical analysis of hill's slopes areas in heritage town of Berati, Albania. *Period. Polytech. Civ.* **2016**, *60*, 61–73. [CrossRef]
2. Tiwari, B.; Ajmera, B.; Dhital, S. Characteristics of moderate to large scale landslides triggered by the Mw 7.8 2015 Gorkha earthquake and its aftershocks. *Landslides* **2017**, *14*, 1297–1318. [CrossRef]
3. Tang, M.; Xu, Q.; Huang, R. Site monitoring of suction and temporary pore water pressure in an ancient landslide in the Three Gorges reservoir area, China. *Environ. Earth Sci.* **2015**, *73*, 5601–5609. [CrossRef]
4. Yin, Y.; Huang, B.; Wang, W.; Wei, Y.; Ma, X.; Ma, F.; Zhao, C. Reservoir-induced landslides and risk control in Three Gorges Project on Yangtze River, China. *J. Rock Mech. Geotech. Eng.* **2016**, *8*, 577–595. [CrossRef]
5. Li, S.; Xu, Q.; Tang, M.; Iqbal, J.; Liu, J.; Zhu, X.; Liu, F.; Zhu, D. Characterizing the spatial distribution and fundamental controls of landslides in the three gorges reservoir area, China. *Bull. Eng. Geol. Environ.* **2019**, *78*, 4275–4290. [CrossRef]
6. Yin, Y.; Wang, H.; Gao, Y.; Li, X. Real-time monitoring and early warning of landslides at relocated Wushan Town, the Three Gorges Reservoir, China. *Landslides* **2010**, *7*, 339–349. [CrossRef]
7. Du, J.; Yin, K.; Lacasse, S. Displacement prediction in colluvial landslides, Three Gorges Reservoir, China. *Landslides* **2013**, *10*, 203–218. [CrossRef]
8. Huang, D.; Gu, D.; Song, Y.; Cen, D.; Zeng, B. Towards a complete understanding of the triggering mechanism of a large reactivated landslide in the Three Gorges. *Reservoir. Eng. Geol.* **2018**, *238*, 36–51. [CrossRef]
9. Deng, Q.L.; Fu, M.; Ren, X.W. Precedent long-term gravitational deformation of large scale landslides in the Three Gorges reservoir area, China. *Eng. Geol.* **2017**, *221*, 170–183. [CrossRef]
10. Li, S.L.; Xu, Q.; Tang, M.G.; Li, H.J.; Yang, H.; Wei, Y. Centrifuge modeling and the analysis of ancient landslides subjected to reservoir water level fluctuation. *Sustanability* **2020**, *12*, 2092. [CrossRef]

11. Li, Y.R.; Mo, P. A unified landslide classification system for loess slopes: A critical review. *Geomorphology* **2019**, *340*, 67–83. [CrossRef]
12. Marin, R.J.; Velásquez, M.F. Influence of hydraulic properties on physically modelling slope stability and the definition of rainfall thresholds for shallow landslides. *Geomorphology* **2020**, *351*, 106976. [CrossRef]
13. Bhardwaj, A.; Wasson, R.J.; Ziegler, A.D.; Chow, W.T.L.; Sundriyal, Y.P. Characteristics of rain-induced landslides in the Indian Himalaya: A case study of the Mandakini Catchment during the 2013 flood. *Geomorphology* **2019**, *330*, 110–115. [CrossRef]
14. Vassallo, R.; Grimaldi, G.M.; Di, M.C. Pore water pressures induced by historical rain series in a clayey landslide: 3D modelling. *Landslides* **2015**, *12*, 731–744. [CrossRef]
15. Tang, H.M.; Li, C.D.; Hu, X.L. Deformation response of the Huangtupo landslide to rainfall and the changing levels of the Three Gorges Reservoir. *Bull. Eng. Geol. Environ.* **2014**, *74*, 933–942. [CrossRef]
16. Tang, H.M.; Li, C.D.; Hu, X.L. Evolution characteristics of the Huangtupo landslide based on in situ tunneling and monitoring. *Landslides* **2015**, *12*, 511–521. [CrossRef]
17. Huang, F.M.; Huang, J.S.; Jiang, S.H.; Zhou, C.B. Landslide displacement prediction based on multivariate chaotic model and extreme learning machine. *Eng. Geol.* **2017**, *218*, 173–186. [CrossRef]
18. Xu, S.L.; Niu, R.Q. Displacement prediction of Baijiabao landslide based on empirical mode decomposition and long short-term memory neural network in the Three Gorges area, China. *Comput. Geosci.* **2018**, *111*, 87–96. [CrossRef]
19. Salciarini, D.; Fanelli, G.; Tamagnini, C. A probabilistic model for rainfall-induced shallow landslide prediction at the regional scale. *Landslides* **2017**, *14*, 1731–1746. [CrossRef]
20. Hou, F.; Lai, Y.M.; Liu, E.L.; Luo, H.W.; Liu, X.Y. A creep constitutive model for frozen soils with different contents of coarse grains. *Cold Reg. Sci. Technol.* **2018**, *145*, 119–126. [CrossRef]
21. Tong, L.; Wang, Y.H. DEM simulations of shear modulus and damping ratio of sand with emphasis on the effects of particle number, particle shape, and aging. *Acta Geotech.* **2015**, *10*, 117–130. [CrossRef]
22. Tsiggions, C.; Zeghal, M. A micromechanical analysis of the effects of particle shape and contact law on the low-strain stiffness of granular soils. *Soil Dyn. Earthq. Eng.* **2019**, *125*, 105693. [CrossRef]
23. Enomoto, T. Effects of grading and particle characteristics on small strain properties of granular material. *Soil Found.* **2016**, *56*, 745–750. [CrossRef]
24. Liu, X.Y.; Zou, D.G.; Liu, J.M. Experimental study to evaluate the effect of particle size on the small strain shear modulus of coarse-grained soils. *Measurement* **2020**, *163*, 107954. [CrossRef]
25. Chang, D.; Lai, Y.M.; Gao, J.Q. An investigation on the constitutive response of frozen saline coarse sandy soil based on particle breakage and plastic shear mechanisms. *Cold Reg. Sci. Technol.* **2019**, *159*, 94–105. [CrossRef]
26. Won, J.M.; Park, J.H.; Choo, H.W.; Burns, S. Estimation of saturated hydraulic conductivity of coarse-grained soils using particle shape and electrical resistivity. *J. Appl. Geophys.* **2019**, *167*, 19–25. [CrossRef]
27. Wang, J.; Liu, F.Y.; Wang, P.; Cai, Y.Q. Particle size effects on coarse soil-geogrid interface response in cyclic and post-cyclic direct shear tests. *Geotext. Geomembr.* **2016**, *44*, 854–861. [CrossRef]
28. Wang, S.; Wang, J.E.; Wu, W.; Cui, D.S. Creep properties of clastic soil in a reactivated slow-moving landslide in the Three Gorges Reservoir Region, China. *Eng. Geol.* **2020**, *267*, 105493. [CrossRef]
29. Deng, Q.L.; Wang, X.P. Growth history of Huangtupo landslide: Down-slope overlapping-landsliding -modification. *Earth Sci. J China Univ. Geosci.* **2000**, *25*, 44–50. (In Chinese)
30. Baiocchi, C.; Comincioli, V.; Magenes, E.; Pozzi, G.A. Free boundary problems in fluid flow through porous media: Existence and uniqueness theorems. *Ann. Mat. Pur. Appl.* **1973**, *97*, 1–82. [CrossRef]
31. Li, C.; Tang, H.M.; Han, D.W. Exploration of the creep properties of undisturbed shear zone soil of the Huangtupo landslide. *Bull. Eng. Geol. Environ.* **2019**, *78*, 1237–1248. [CrossRef]
32. Yuan, W.; Li, J.X.; Li, Z.H. A strength reduction method based on the Generalized Hoek–Brown (GHB) criterion for rock slope stability analysis. *Comput. Geotech.* **2020**, *117*, 103240.